Activation of NMDA Receptors in Rat Dentate Gyrus Granule Cells by Spontaneous and Evoked Transmitter Release

Nils Ole Dalby and Istvan Mody

Departments of Neurology and Physiology, The David Geffen School of Medicine at UCLA, Los Angeles, California 90095-1769

Dalby, Nils Ole and Istvan Mody. Activation of NMDA receptors in rat dentate gyrus granule cells by spontaneous and evoked transmitter release. *J Neurophysiol* 90: 786–797, 2003; 10.1152/jn.00118.2003. Activation of *N*-methyl-D-aspartate (NMDA) receptors by synaptically released glutamate in the nervous system is usually studied using evoked events mediated by a complex mixture of AMPA, kainate, and NMDA receptors. Here we have characterized pharmacologically isolated spontaneous NMDA receptor-mediated synaptic events and compared them to stimulus evoked excitatory postsynaptic currents (EPSCs) in the same cell to distinguish between various modes of activation of NMDA receptors. Spontaneous NMDA receptor-mediated EPSCs recorded at 34°C in dentate gyrus granule cells (DGGC) have a frequency of 2.5 ± 0.3 Hz and an average peak amplitude of 13.2 ± 0.8 pA, a 10–90% rise time of 5.4 ± 0.3 ms, and a decay time constant of 42.1 ± 2.1 ms. The single-channel conductance estimated by nonstationary fluctuation analysis was 60 ± 5 pS. The amplitudes (46.5 ± 6.4 pA) and 10–90% rise times (18 ± 2.3 ms) of EPSCs evoked from the entorhinal cortex/subiculum border are significantly larger than the same parameters for spontaneous events (paired *t*-test, $P < 0.05$, $n = 17$). Perfusion of 50 μM D(−)-2-amino-5-phosphonopentanoic acid blocked all spontaneous activity and caused a significant baseline current shift of 18.8 ± 3.0 pA, thus identifying a tonic conductance mediated by NMDA receptors. The NR2B antagonist ifenprodil (10 μM) significantly reduced the frequency of spontaneous events but had no effect on their kinetics or on the baseline current or variance. At the same time, the peak current and charge of stimulus-evoked events were significantly diminished by ifenprodil. Thus spontaneous NMDA receptor-mediated events in DGGC are predominantly mediated by NR2A or possibly NR2A/NR2B receptors while the activation of NR2B receptors reduces the excitability of entorhinal afferents either directly or through an effect on the entorhinal cells.

INTRODUCTION

N-methyl-D-aspartate (NMDA) receptors are localized in the postsynaptic membrane (Chen and Diamond 2002; Diamond 2001; Isaacson 1999; Kullmann et al. 1999; Momiyama 2000; Rumbaugh and Vicini 1999; Sattler et al. 2000; Tovar and Westbrook 1999) and at certain presynaptic terminals (Breukel et al. 1998; Milner and Drake 2001; Paquet and Smith 2000; Woodhall et al. 2001). This anatomical arrangement is also reflected by NMDA receptor subtype heterogeneity. Thus the five NMDA-receptor subunits, NR1 (8 isomers, A-H) and the four NR2 subunits (A-D), co-assemble into functional NMDA receptors, presumably in the stoichiometry of two NR1 glycine-binding and two NR2 glutamate-binding subunits (Laube

et al. 1998). In cell culture, synaptic NR2A-containing receptors appose presynaptic release sites, whereas NR2B-containing receptors are located predominantly outside the postsynaptic density (Tovar and Westbrook 1999). The latter subunits also appear to be present on presynaptic terminals of entorhinal cortex (EC) neurons in acutely prepared brain slices (Woodhall et al. 2001). There is evidence from in vitro studies of heterotrimeric NMDA receptors such as NR1/NR2A/NR2B subunit combinations (Brimecombe et al. 1997; Chen et al. 1997; Vicini et al. 1998), but if such receptors are expressed in vivo (Pina-Crespo and Gibb 2002), their subcellular localization is unknown.

NR2A and NR2B receptor subunits are coupled through different C-terminal domains to distinct second-messenger pathways (Chan and Sucher 2001; Krupp et al. 2002; Lieberman and Mody 1994; Sattler et al. 2000), which in addition to their separate localizations serve to diverge NMDA receptor signaling. For example, extrasynaptic NR2B, but not synaptic NR2A receptors, induce long-term genomic translational effects through activation of the cAMP-responsive binding protein (Hardingham et al. 2002). Whenever NMDA receptors in the same intact synaptic structure can be expressed on the presynaptic terminal and both in- and outside of the postsynaptic density, it complicates the experimental design aimed at distinguishing between the roles of the different receptors. Due to the poor signal-to-noise ratio of spontaneous NMDA receptor-mediated events, stimulus-evoked events are the usual choice for characterizing the activation of postsynaptic NMDA receptors. A major difference between stimulus-evoked and spontaneous events is that spontaneous events are monosynaptic in origin, causing a relatively limited spillover of transmitter to extrasynaptic receptors or neighboring postsynaptic sites. In contrast, events evoked by stimulation of afferent fibers can be polysynaptic and may be due to the simultaneous activation of neighboring release sites, causing considerable spillover activating extrasynaptic receptors or neighboring synapses (Barbour and Hausser 1997; Diamond 2001; Kullmann et al. 1999; Lozovaya et al. 1999). To further our understanding of this anatomical and functional receptor heterogeneity in an intact system of synaptical structures, it is necessary to establish physiological methods to characterize the mode of activation of NMDA receptors at synapses. The purpose of the present study was twofold: first we set out to distinguish the properties of spontaneous NMDA receptor-mediated events in dentate gyrus

---

Address for reprint requests: I. Mody, Depts. of Neurology and Physiology, The David Geffen School of Medicine at UCLA, 710 Westwood Plaza, RNRC 3-155, Los Angeles, CA 90095-1769 (E-mail: mody@ucla.edu).

granule cells including the underlying single-channel conductance. Second, we compared spontaneous and stimulus-evoked events recorded in the same cell to distinguish between the activation of NMDA receptor subtypes by evoked and spontaneously released glutamate.

METHODS

Slice preparation

Rat brains were obtained from 8 to 10 wk old Sprague Dawley rats (Harlan). Briefly, rats were decapitated after pentobarbital (75 mg/kg ip) anesthesia, and the head was quickly chilled. The brain was then rapidly dissected out in artificial cerebrospinal fluid (ACSF) containing (in mM): 126 NaCl, 2.5 KCl, 2 CaCl$_2$, 2 MgCl$_2$, 26 NaHCO$_3$, 1.25 NaH$_2$PO$_4$, 10 D-glucose, 0.3 ascorbate, and 1.0 pyruvic acid. The brain was glued with cyanocryalate to the platform of a Leica 1000 VS microtome and cut into 350-μm-thick horizontal slices. Osmolarity of ACSF was 300 $\pm$ 10 mosM, pH 7.4 $\pm$ 0.1, and kynurenic acid (3 mM) was added to the ACSF used in the dissection procedures only. Slices were hemi-sected and stored in a chamber with continuously carbogenated ACSF for 1–4 h at 32°C before being individually transferred to a recording chamber. NMDA responses were pharmacologically isolated in a modified ACSF (ACSF$_{NMDA}$) containing as described above but with only 5 μM MgCl$_2$ and with the following compounds added (in μM) 10 DNQX, 30 picrotoxin, and 10 D-serine. For field and whole cell recordings, we used slices that were located approximately between 3.5 and 6.5 mm dorsal to the interaural line (IAL, also see Fig. 8A). In a separate set of experiments we also recorded bursts in whole cell and field configuration in slices positioned approximately between 2 and 3 mm above the interaural line (see Fig. 8B) (Paxinos and Watson 1998). During the field recordings of these ventral slices, a cut was made in the slice by a manipulator-controlled micro-scalpel to sever the entorhinal cortex from the subiculum and dentate gyrus, thus transecting the perforant path.

Field potential recordings

During recordings slices were held in place on lens tissue paper by small platinum weights and continuously perfused with carbogenated ACSF$_{NMDA}$ at 34–35°C at a flow rate of 1.5–2 ml/min in a chamber with an internal carbogenated and humidified atmosphere. A bipolar tungsten stimulating electrode was placed in the perforant path/angular bundle immediately before crossing the hippocampal fissure and set to deliver a 40-μs stimulus every 30 s. A recording glass electrode filled with ACSF$_{NMDA}$ prepared as described below for whole cell recordings was placed in the outer molecular layer of the dentate gyrus. Current intensities for stimulation were set to evoke field potentials of $\geq$0.4 mV peak amplitude, i.e., ~60% of the stimulus intensity required to evoke maximal peak responses.

Whole cell voltage-clamp recordings

Recording electrodes were made of borosilicate glass capillaries with an inner filament (1.10 mm ID, 1.5 mm OD, Garner glass) and pulled on a two-stage Narishige PP-83 puller or Zeitz horizontal puller (resistances: 5–8 MΩ). Intracellular solution (ICS) contained (in mM) 135 CsCl, 4 NaCl, 2 MgCl$_2$, 10 N-2-hydroxyethylpiperazine-N'-2-ethanesulphonic acid (HEPES), 0.05 EGTA, 5 QX-314, 5 tetraethylammoniumchloride (TEA), 2 Mg-ATP, 0.5 Na$_2$-GTP. The pH of the ICS was adjusted to 7.2 with CsOH and its osmolarity was 285–290 mosM. Type of chamber and ACSF$_{NMDA}$ were similar for field and whole cell recordings. A stimulating electrode was placed in the angular bundle at the border of entorhinal cortex and the subiculum and set to deliver a stimulus every 20 s. Dentate gyrus granule cells were recorded using blind-patching, i.e., by lowering patch electrodes down through the granule cell layer while monitoring responses to 5-mV test pulses (Staley et al. 1991). Seals ($>$7 GΩ) were formed by applying gentle suction to patch pipettes. Whole cell currents were amplified and low-pass filtered (2 kHz, 8-pole bessel) using an Axopatch 200A amplifier (Axon Instruments, Burlingame, CA) and 75% compensated for series resistance. Cells were held for a period of $\geq$25 min during which series resistance and capacitance were monitored every 3–4 min. After 10-min recording of baseline spontaneous and evoked events, ifenprodil (10 μM) was added to the perfusate and an additional 10 min were recorded after its addition. Cells in which series resistance or capacitance deviated by $>$50% from initial values were excluded from analysis. Also, cells with series resistances $>$18 MΩ at any time during the recording were excluded from analysis.

Establishing the time course of evoked NMDA EPSCs

The true synaptic conductance was determined by the method of charge recovery of timed evoked events during a series of predetermined voltage jumps (Hausser and Roth 1997; Pearce 1993). The Strathclyde whole cell program V3.2.6 (courtesy of J. Dempster) was used to generate voltage jumps from the reversal potential to $-$60 mV. Three to four repetitions of a series of 11 trials with stimulation times from $-$150 to $+$100 ms relative to the voltage jump were recorded and traces uncontaminated by spontaneous events were averaged and subtracted from traces without stimulation. The charge recovery was determined as the area-over-curve (AOC) of subtracted traces and plotted against time relative to the voltage jump. A single exponential was fitted to the curve from 150 to 15 ms before the voltage jump and the time constant compared with the time constant from events recorded 100 ms after the voltage jump.

Data sampling

Field DC potentials were amplified 100 times through the headstage and again 10 times through a BrownLee 440 precision amplifier (San Jose, CA) and band-pass filtered (0.1–2 kHz) before digitization and storage on a Pentium-processor-based PC using the in-house designed event detection and analysis (EVAN) software package (www.EV-AN.Thotec.com). Analog whole cell recordings were low-pass filtered at 2 kHz ($-$3 dB, 8-pole Bessel, Frequency Devices 9002) and digitized on-line at 8 kHz. Back-ups of field and whole cell recordings were digitized through a Neurocorder (Neurodata) at 88 kHz and stored on videotape.

Drugs

The sources of drugs were as follows: ifenprodil (Tocris, stock dissolved in DMSO to100 mM), D-APV (Tocris), R-($-$)-3-(2-carboxypiperazin-4-yl)propanephosphonic acid (D-CPP, Tocris), lidocaine N-ethyl bromide (QX-314, Alomone lab), tetraethylammonium-chloride (TEA, Sigma), 6,7-dinitroquinoxaline-2,3(1H,4H)-dione (DNQX, Sigma), picrotoxin (Sigma) and D-serine (Sigma).

Detection, selection, and analysis of NMDA receptor-mediated events

NMDA receptor-mediated events were identified in 300-s-long continuous recordings based on the following criteria: a baseline (BL) of 50 ms followed by a downward deflection of $\geq$3 $\times$ BL SD (σ_{BL}) lasting for $>$0.5 ms was identified as an event and periods of 100 ms before and 300 ms after were sampled around the detection time. A dead time of 15 ms and baseline standard deviation (SD) criteria of $\sigma_{BL} <$ 10 pA were used to select events only once. Events were counted for frequency measurement but rejected for further analysis if any other events were detected in $-$50 ms prior or 250 ms after the detection point for a given event. Gaussian distributions were fitted to 10–90% RT, peak, 67% decay time, and total charge carried by the event (AOC, from detection till $+$250 ms). The number of Gaussians

in the overall distribution for each parameter was determined by the F value for two distributions with n and $n + 1$ peaks by $F = [(SS_n - SS_{n+1})/(f_n - f_{n+1})]/(SS_n/f_{n+1})$ and the associated P value by $P = 1 - invf[F, (f_n - f_{n+1}), f_{n+1}]$, using $P < 0.05$ as level of significance where SS is sum of squares, f is degrees of freedom, and invf is the inverse of the F distribution function. The inter-event intervals were binned in log-scaled bins and the mean (μ) for the exponential distribution was determined by fitting the function $N = l*exp\{\ln (x/\mu) - exp[\ln (x/\mu)]\}$ to the data. The weighted decay time constant ($\tau_{weighted}$) of spontaneous and evoked events was estimated from the mean EPSC trace by dividing the AOC measured from the peak (AOC_{peak}) by the peak amplitude or by fitting a single exponential to the 20–80% decay-phase. An estimate of mean-channel conductance, γ, was obtained by nonstationary fluctuation analysis (NSFA) applied to groups of 60–90 events comprised in the major Gaussian (mean $\pm$ SD) of the peak distribution. The variance around the mean in the period 5 $\sim$ 240 ms after the mean peak were divided into 25 bins and plotted against the mean single-channel current and fitted with the relation $\sigma^2 = i \cdot I - I^2/N - \sigma_{BL}^2$ in which σ^2 is the bin-variance of traces around the mean, σ_{BL}^2 is the baseline variance, i is the single-channel current and I is the mean current passed by the ensemble of N channels (De Koninck and Mody 1994). The conductance is given by $\gamma = i/(V_m - V_{rev})$ in which V_m is the membrane (holding) potential and V_{rev} is the reversal potential of NMDA receptors in this preparation. A $V_{rev} = 3$ mV was obtained from I-V plots of evoked events at holding potentials ranging from -60 to $+40$ mV. An estimate of the average number of channels open at the peak is given by the ratio of peak current to the single-channel current, i, obtained by NSFA. Spectral analysis was performed on 39 discontinuous 4.096-s-long (32,768 points) traces (low-pass filtered at 3 kHz, 8-pole Bessel) of a baseline period and a similar period recorded during D-APV or D-CPP. The data were Blackman-windowed and the one-sided power spectrum for each trace was obtained by fast Fourier transformation (FFT) and all FFTs averaged for each period. The subtracted power spectrum (baseline – APV or CPP) was plotted in a log-log diagram and the corner-frequencies, f_c, were obtained by fitting the data to a Lorentzian of the general form: $S(f) = \sum_{1}^{n} S(0)_n/(1 + (f/f_{c_n})^2)$, in which $S(0)$ is the lowest frequency noise intercept of the spectral density and f_c is the corner-frequency. The corner frequencies relate to the relaxation time constant of a single exponential by $\tau = 1/(2\pi \cdot f_c)$.

RESULTS

Characterization of spontaneous NMDA receptor-mediated events

Pharmacological isolation of NMDA receptor-mediated events recorded at 34–35°C was obtained through the removal of currents through $GABA_A$, AMPA, and kainate receptors, the application of the glycine-site agonist D-serine, and recording in a low Mg^{2+}-medium to relieve the voltage-dependent block of NMDA receptors. Postsynaptic Na^+ and K^+ channels were blocked by QX-314, Cs, and TEA in the intracellular solution. While holding cells at -60 mV, the holding current decreased to a stable value (-35 ± 10.7 pA, $n = 17$, Table 1) 3–5 min after establishment of the whole cell configuration. Application of 50 μM D-APV completely blocked the synaptic events, decreased the baseline holding current by 18.8 ± 3 pA ($n = 5$) and decreased the SD of the baseline current (Fig. 1, *A–C*). Therefore the spontaneous events were mediated solely by NMDA receptors while the openings of NMDA channels also significantly contributed to the baseline variance. NMDA receptor-mediated events are characterized by slow rise time, long decay time, and a mean peak of -13.2 ± 0.8 pA and

TABLE 1. *NMDA Receptor-mediated events, granule cells*

	Spontaneous Events	Evoked Events
10–90% RT, ms	5.4 $\pm$ 0.3	18.0 $\pm$ 2.3*
Peak current, pA	-13.2 ± 0.8	-46.5 ± 6.4*
Eventarea (AOC) fC	-615 ± 39	-3806 ± 942*
$T_{weighted}$ ($AOC_{peak}/Peak_{peak}$)	39.6 $\pm$ 2.2	ND
T_{fitted}	41.1 $\pm$ 2.9	51.7 $\pm$ 6.3†
Baseline current, pA	-35.3 ± 10.7	ND
Baseline variance, pA^2	7.5 $\pm$ 1.0	ND
Conductance, pS	60 $\pm$ 5	ND
Channels open at peak	$\sim$4	ND
Interevent interval, tau, s	0.39 $\pm$ 0.06	20

Values are means $\pm$ SE of 17 granule cells. NMDA, N-methyl-D-aspartate; ND, not determined. * Significant difference between the control and ifenprodil (10 μM) period (paired t-test, $P < 0.05$). † $P = 0.10$.

baseline SD (σ_{BL}) $\sim$2.7 pA (Table 1, means $\pm$ SE of 17 granule cells). A set signal to noise ratio of 3 was used as detection limit (ratio of lowest peak detected and σ_{BL}). Distributions of peak amplitude and of rise-time were in all cells best fitted to two or three Gaussian distributions (Figs. 2*B* and 3*B*). Similarly, 67% decay times were best described by two or three Gaussian distributions (Fig. 3*C*), whereas in the majority of cells the distribution of charge carried by the events (AOC, fC) was adequately described by a single-Gaussian with a mean of -615 ± 39 (SE) fC (Fig. 2*C*, Table 1). Overall, there is an apparent proportionality among rise time, 67% decay time and amplitude of the events (Fig. 3*D*).

Spectral analysis of 160-s-long traces (average of 39 traces of 4.096 s length) in four cells resolved two corner frequencies in the range 2.6–3.2 and 210–288 Hz, corresponding to exponential relaxation time constants of 49–61 and 0.6–0.8 ms respectively. The low-frequency component is in good agreement with the decay time constant of the average event recorded during control conditions (Fig. 4, *A* and *B*), while the latter frequency most likely reflects the average lengths of openings of NMDA channels in these neurons (Lieberman and Mody 1994).

NMDA channel conductance

An estimate of the synaptically activated NMDA-channel conductance was obtained through nonstationary fluctuation analysis (NSFA, Fig. 2*D* and Table 1). To reduce the variation due to possible differences in synaptic size, number of channels, and dendritic filtering (De Koninck and Mody 1994; Traynelis et al. 1993), NSFA was performed on 60–90 events selected around the mean $\pm$ 1 SD in the dominant Gaussian of the peak-amplitude distribution (Fig. 2*B*, shaded area). Arguably, scaling of individual peaks to the mean peak before subtraction would be preferred to account for the variable number of channels shaping the individual event if the p_{open} is high. However, NMDA channels possess a high intrinsic variance in the time from binding of agonist to first opening (Lester et al. 1990) and a relatively low p_{open}. Therefore, even after selecting events as described in the preceding text, a significant bias is introduced with peak scaling because of differing peak times. Without peak scaling, the analysis of 17 granule cells yielded an estimated average unitary current $i = -3.42$ pA corresponding to a conductance, $\gamma = 60 \pm 5$ pS (Table 1). With an average peak amplitude of -13.2 pA (Table 1), this led
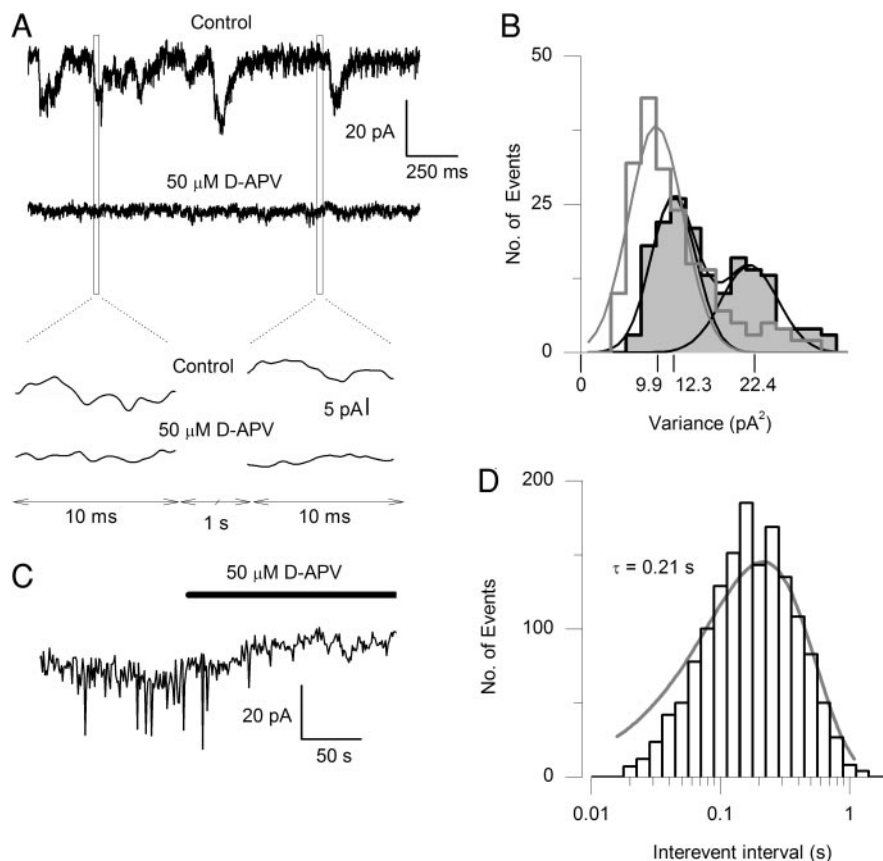
FIG. 1. Whole cell *N*-methyl-D-aspartate (NMDA) receptor-mediated spontaneous currents recorded from rat dentate gyrus granule cells. *A*: sensitivity to D(−)-2-amino-5-phosphonopentanoic acid (D-APV). *Bottom*: baseline holding current and variance are calculated by sampling 10-ms traces at 1-Hz frequency throughout the recording. *B*: the distribution of the baseline variance of these 10-ms traces. In control conditions, some of the systematically sampled 10-ms traces will fall on the rise or decay phases of excitatory postsynaptic currents (EPSCs) giving rise to a high variance (2nd peak in gray-shaded sum of Gaussian distributions). The application of D-APV (50 μM) significantly reduced baseline variance (peak in nonshaded single-Gaussian distribution) indicating the presence of NMDA receptor-mediated openings. *C*: blocking NMDA receptors by APV or R-(−)-3-(2-carboxypiperazin-4-yl)propanephosphonic acid (CPP) caused a significant decrease in the holding current of ~19 pA. *D*: a log-binned plot of interevent intervals is shown to follow an exponential distribution (line) with a tau corresponding to an average frequency of 4.8 Hz.

to an estimate of approximately four NMDA channels open at the peak of the average spontaneous NMDA EPSC.

Comparison of evoked and spontaneous events

Events were evoked by a stimulating electrode in the perforant path at the subiculum-entorhinal cortex border (Fig. 5*A*, site 1) or in the hippocampal fissure at the site from which field potentials were evoked (Fig. 5*B*, site 2) every 20 s. Individual slices were stimulated at one site only. Events evoked from both sites had longer rise-times and larger peak-currents and AOC than the spontaneous events (Tables 2 and 3). However, the decay time constant of site-1-evoked events was not significantly larger than that of spontaneous events (paired *t*-test, $n = 17$, $P = 0.10$). Evoked events from stimulation site 2 differed from those evoked from site 1 by higher peak amplitudes and by longer decay time constants, significantly different from that of spontaneous events (table 3, $P < 0.05$, paired *t*-test) recorded during the same period.

Charge recovery of evoked events

Stimulation at site 1 of cells held at +3 mV (the reversal potential of currents through NMDA receptors) did not cause detectable events. By timing the stimulation relative to a jump to a holding potential of −60 mV from the reversal potential, the remaining charge caused by the event can be recovered by the shift to the latter holding potential when corrected for the capacitive current. The charge recovery in a series of 11 trials with stimulation times ranging from −150 to +100 ms relative to the voltage jump is shown in Fig. 6*A*. An event recorded 100

ms after the voltage jump is shown in Fig. 6*B*. The average rise time (RT_{0-100}), for these events of four cells is 16.2 ± 2.4 (SE) ms. The fitted decay time constant, τ is 52.3 ± 6.3 ms. Fitting a single exponential to the charge recovery graph from 150 to 15 ms before the jump (Fig. 6*B*) yields an average time constant of 48.1 ± 7.6 ms.

Effect of ifenprodil on spontaneous and evoked events in whole cell recordings

Ifenprodil (10 μM, in final 0.1 ‰ DMSO) had no effect on RT 10–90%, 67% decay time, peak-current, weighted or fitted tau measured in the decay phase of EPSC's charge carried by the events (AOC, pA*ms), baseline holding current, baseline SD, or unit channel conductance of spontaneous events (Table 2, Fig. 7*A–F*). However, ifenprodil significantly reduced the frequency of spontaneous events (Table 2, Fig. 7*C*). Evoked events from site 1 recorded simultaneously during the same period had significantly reduced peak currents and AOC (Fig. 7*D*) which was similar for site 2 stimulation (Table 3).

Field potentials

Field potentials of pharmacologically isolated events were evoked with a stimulating electrode in the perforant path close to the hippocampal fissure and to the stratum lacunosum moleculare. With a current stimulation adjusted to yield 60% of the maximal response, field-responses remained stable for >1 h. As seen with evoked events in whole cell configuration, ifenprodil significantly (paired *t*-test, $P < 0.05$, $n = 6$) reduced the peak amplitude and AOC of NMDA receptor-mediated
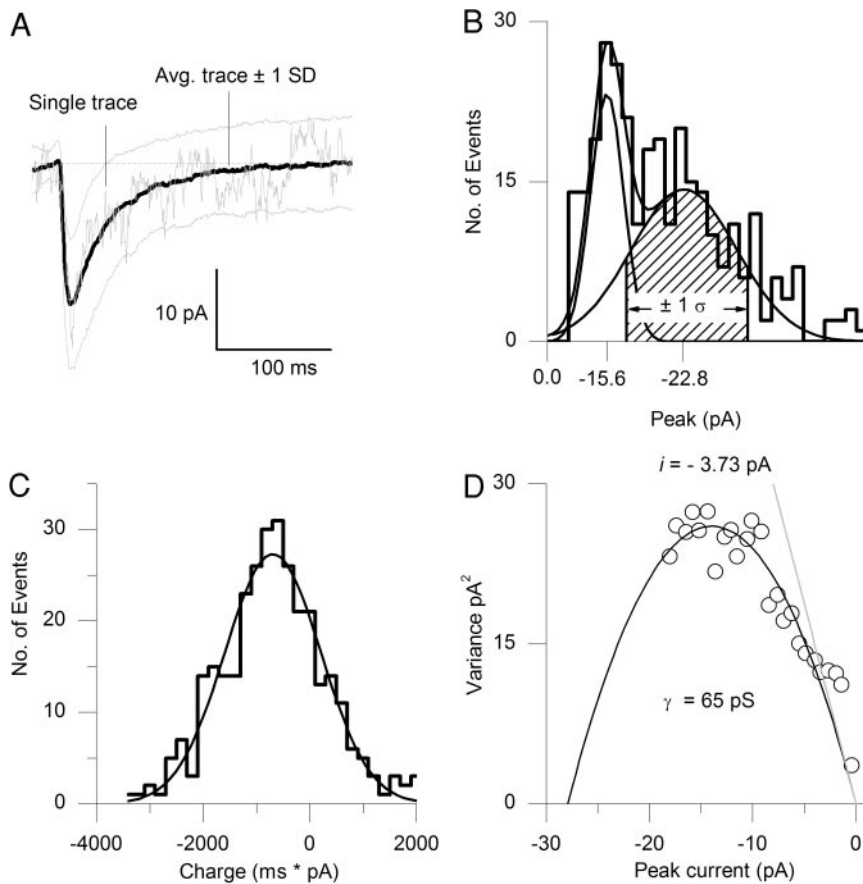
FIG. 2. NMDA receptor-mediated events are characterized by small amplitudes and slow rise and decay times. *A*: a typical event (gray noisy trace) is superimposed on the ensemble average (black smooth trace) ±1 SD (SD, smooth gray traces). *B*: the peak distribution for 320 events for a control cell was best described by the sum of 2 or 3 Gaussian distributions. The shaded area indicates the mean of the dominant Gaussian ±1 SD, the criteria used for selecting 60–90 events for the nonstationary fluctuation analysis (NSFA) in *D*. *C*: the charge distribution for the same cell (area over curve, AOC, pA*ms = fC), was typically well described by a single Gaussian distribution. Note that a considerable number of events had AOC >0 as can be expected from the average ±1 SD shown in *A*. *D*: plot of the baseline variance subtracted variance as a function of mean current is well fitted to the parabolic relation $\sigma_I^2 = i*I - I^2/N$ (see text for details). The value obtained from the fit for the single-channel current is 3.72 pA indicated on the fit as the slope of the tangent to the fit at 0 variance and current.
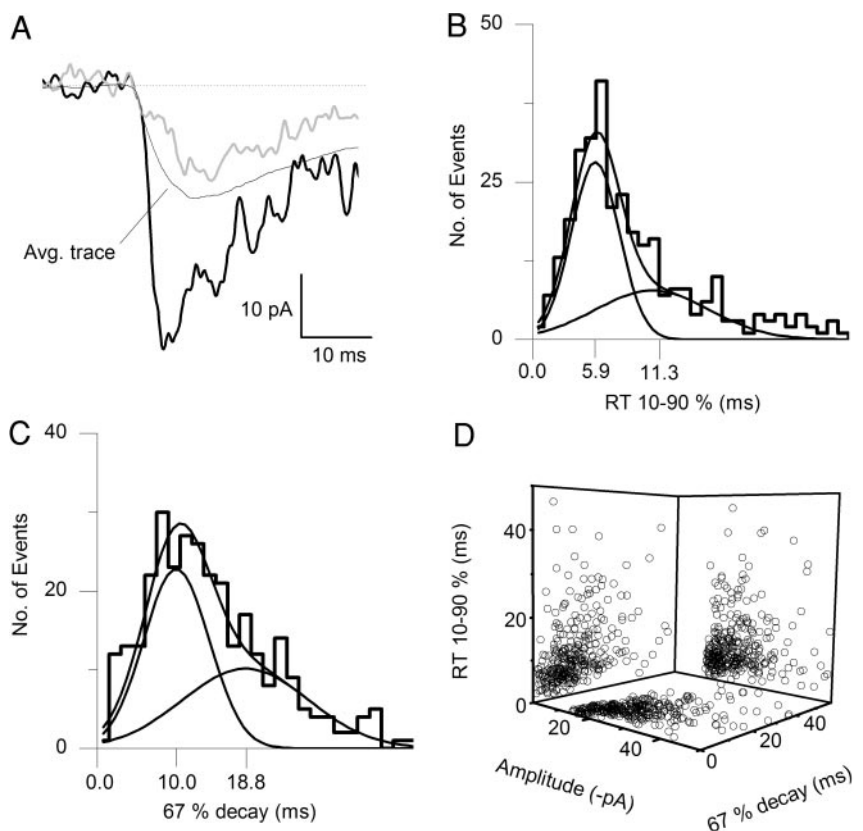
FIG. 3. Characteristics of NMDA receptor-mediated events. *A*: magnification of 2 single noisy traces around the ensemble average (smooth trace). The 2 events have different peak, rise, and decay times. *B* and *C*: the distributions for 10–90% rise times and 63% decay times, respectively, from the same cell in Fig. 2. Typically, 2 different rise times could be distinguished with a mean ~5 and 11 ms and also decay times ~10 and 20 ms. *D*: graphical illustration of the relation among peak amplitude, 10–90% rise time, and 63% decay time for the 320 events.
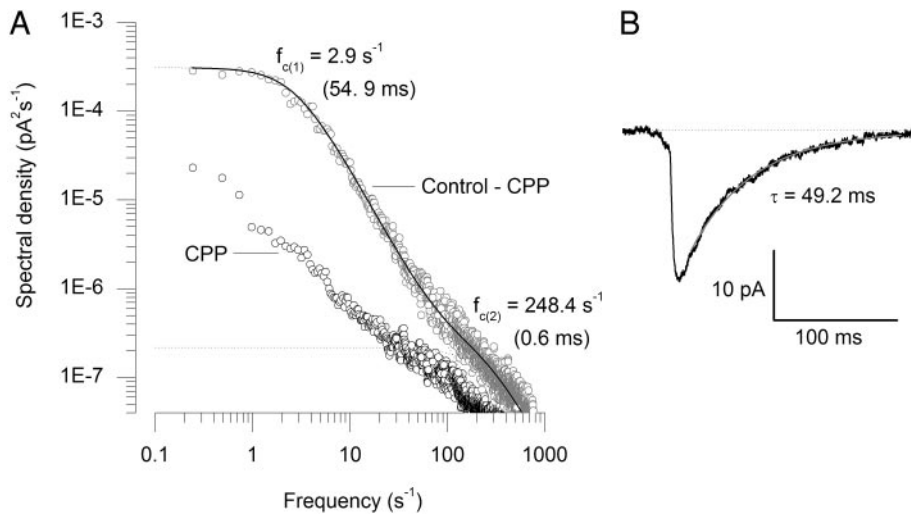
FIG. 4. Average power-spectra of 39 continuous 4.1-s long traces (160-s-long total) has a corner frequency comparable to the decay time constant of spontaneous events recorded in the same period. *A*: the power spectrum of baseline minus the power spectrum during CPP fitted to a double Lorentzian (see METHODS) has 2 characteristic corner frequencies of 2.9 and 248.4 Hz which translate into time constants of 54.9 and 0.6 ms. The spectrum of the CPP trace has less power and no resolvable corner frequency. *B*: average spontaneous event recorded under baseline conditions has a decay time constant of 49.2 ms in good agreement with that of 54.9 ms obtained in the power spectrum (*A*).

field EPSPs. In addition, ifenprodil also reduced the decay time of the field potentials (table 3, $n = 6$, $P < 0.05$, paired *t*-test, 5–10 min after application).

Dorsoventral differences in synaptic bursting of granule cells

We identified a sharp transition zone along the dorsoventral axis separating two regions of the hippocampus with different levels of synaptic bursting of granule cells. Ventral to this zone, lying ~3 mm above the interaural line (Fig. 8*A*), five of five granule cells displayed spontaneous bursts (2–3/min) with peak currents ~2 orders of magnitude larger than the mean peak current of normal events in ventral and dorsal slices (Fig. 8*C*). This type of large event was never observed in dorsal slices. The presence of spontaneous field events with similar

frequency (2–3/min) recorded in the same region is most likely a reflection of intracellular bursts. Evoked field and whole cell events in this ventral region were characterized by double peaks, 2–300 ms apart, both sensitive to inhibition by D-APV (not shown) and ifenprodil (Fig. 8*D*). In whole cell configuration, these bursts reversed polarity when recorded at +40 mV (Fig. 8, *C* and *D*), excluding the possibility of unclamped Ca^{2+} currents as the underlying mechanism. In field recordings, we investigated the possibility that the double peaks observed were due to reverberating activity or antidromic stimulation between entorhinal cortex and dentate gyrus by cutting away the entorhinal cortex (Fig. 8*B*) while recording field potentials. In each of the four slices studied, the double peak disappeared after a cut severing the entorhinal cortex from the dentate gyrus (Fig. 8*F*).
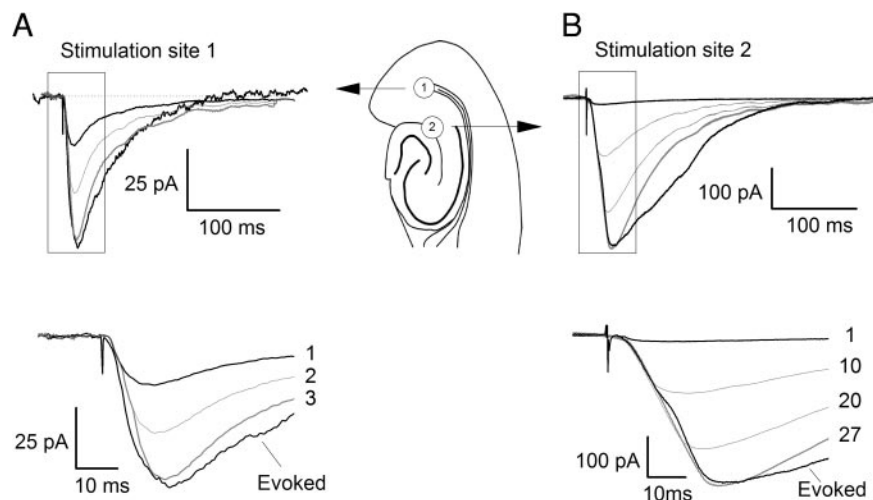

FIG. 5. Characteristics of events evoked from 2 different stimulation sites. Individual slices were stimulated at 1 site only. In the center, a horizontal section depicts the 2 sites of stimulation: site 1 being in the angular bundle at the border of the entorhinal cortex (EC) and the subiculum and site 2 in the hippocampal fissure where the perforant path enters the molecular layer. *A*: whole cell recording of events evoked from stimulation site 1. These evoked events were on average 3–4 times (peak) larger than spontaneous events recorded in the same cell but were not significantly different with respect to decay time constant (Table 2). The average spontaneous event is shown (small event) with evoked event (large noisy trace). The 3rd (large, smooth) trace is constructed of by adding 3 staggered spontaneous events so that rise time and peak of the evoked event is matched (see *B*). The decay time constant of the evoked event is 49.3 ms, and the staggered, constructed event is 43.2 ms. *B*: whole cell recordings of events evoked from site 2. These events have significantly longer decay time constants than the spontaneous events recorded at the same time in the same cell (Table 3). The composite event is constructed by the addition of 27 staggered spontaneous events with the criteria to match rise time and peak yielding a decay time constant of 57.1 ms, compared with 102.2 ms for the evoked event. In this case (compare with *A*), the composite event does not approach the decay kinetics of the evoked event.

TABLE 2. *Stimulation in subiculum/EC, effect of ifenprodil*

	Spontaneous Events		Evoked Events	
	Control	Ifenprodil	Control	Ifenprodil
Peak*0.8/20–80% RT	-3.6 ± 0.4	-4.1 ± 0.6	-9.0 ± 3.1	-5.3 ± 1.8
10–90% RT, ms	5.4 ± 0.4	5.2 ± 0.6	18.1 ± 3.7	17.5 ± 3.0
Peak current, pA	-15.7 ± 2.2	-15.5 ± 1.8	-48.3 ± 13.1	$-30.5 \pm 8.3^*$
Eventarea (AOC), fC	-689 ± 68	-722 ± 77	-3885 ± 1394	$-2385 \pm 854^*$
$T_{weighted}$ (AOC/Peak)	50.7 ± 6.4	50.9 ± 6.0	ND	ND
T_{fitted}	44.0 ± 8.4	45.6 ± 9.7	53.5 ± 8.8	70.3 ± 14.4
Baseline current, pA	-47.0 ± 18	-51.0 ± 12	ND	ND
Baseline variance, pA^2	7.1	7.2	ND	ND
Conductance, pS	66 ± 6	69 ± 5	ND	ND
Interevent invl., tau, s	0.23 ± 0.05	$0.45 \pm 0.1^*$	20	20

Values are means $\pm$ SE of 5 cells. * Significant difference between the control and Ifenprodil (10 μM) period (paired *t*-test, $P < 0.05$). Spontaneous and evoked events were monitored simultaneously in the same cell.

DISCUSSION

The activation of NMDA receptors at and around synapses has traditionally been studied by recording stimulus-evoked or spontaneous composite AMPA/kainate and NMDA receptor-mediated EPSCs in which the NMDA component can be identified by its sensitivity to APV or MK-801 (Diamond 2001; Hestrin et al. 1990; Traynelis et al. 1993). Here we characterized the spontaneous and evoked events purely mediated by NMDA receptors in the same cell, which allowed us to discern considerable differences between the activation of NMDA receptors by stimulus evoked and spontaneous glutamate release in hippocampal slices. We characterized the basic parameters of pharmacologically isolated spontaneous NMDA receptor mediated events in rat dentate gyrus granule cells (Figs. 2 and 3, Table 1). We also demonstrated that spontaneous openings of NMDA receptors significantly contribute to the holding current of the cell shown by its sensitivity to D-APV or D-CPP (Fig. 1, *B* and *C*). Furthermore we have established that the NR2B subunit containing NMDA channels do not participate in the shaping of EPSCs activated by spontaneously released transmitter but regulate the frequency of these events (Fig. 7C). In contrast, events evoked in the same cell by stimulating the perforant path were significantly diminished by ifenprodil (Table 2, Fig. 7D), an effect quite similar to that described for NMDA receptor-mediated field-potentials (Gordey et al. 2001). Finally we show that granule cells from ventral brain slices (Fig. 8, *A* and *B*) display spontaneous NMDA receptor-mediated bursts (Fig. 8C) and evoked events (Fig. 8, *D* and *E*, whole cell) that are $\sim$2 orders of magnitude larger than their counterparts recorded in dorsal slices.

Characterization of spontaneous events

The basic characteristics (RT 10–90%, 67% decay time, peak-currents, decay time constant, and channel conductance) have not been previously measured directly from the analysis of spontaneous NMDA receptor-mediated events. In every cell, the distributions of peak amplitudes, 10–90% rise times, and 67% decay time were best described by a sum of 2 or 3 Gaussians (Figs. 2B and 3, *B* and *C*), whereas the charge carried by the event (AOC) was adequately described by a single Gaussian (Fig. 2C).

The decay time constant of 42.1 ± 2.1 ms ($n = 17$, Table 1) corresponds well to the mean activation unit (super-cluster duration) of NMDA channels during a synaptic activation, and we note that it is comparable to the super-cluster duration of NR2A channels after single fast exposure (1 ms) to low glutamate (5–100 nM, $\sim$36 ms) and to the fast component resolved in the response to high glutamate (1 mM, $\sim$70 ms) (Wyllie et al. 1998). Spectral analysis of 4.096-s-long epochs during control perfusion and during perfusion with D-CPP show that the first corner frequency of 2.9 Hz corresponding to a decay time constant of 54.9 ms is in good agreement with the actual observed decay time constant of 49.2 ms (Fig. 4, *A* and *B*). A second corner frequency in the low-millisecond range relates to the channel kinetics of openings during super-cluster duration (events) and also of NMDA channel noise in the baseline and is slightly lower than the mean open time of NMDA channels (1.3 ms) that has been previously described in cell-attached recordings (Lieberman and Mody 1994).

The NMDA receptor subtype expressed in adult rat dentate gyrus granule cells is predominantly NR1, NR2A, and NR2B

TABLE 3. *Stimulation in the hippocampal fissure, effect of ifenprodil*

	Control			Ifenprodil		
	Spontaneous	Evoked	Fields	Spontaneous	Evoked	Fields
10–90% RT, ms	$6.8 \pm 0.4^{(1*)}$	$17.3 \pm 4.1^{(13*)}$	12.2 ± 2.9	$6.7 \pm 0.4^{(2*)}$	$16.3 \pm 3.2^{(2*)}$	11.9 ± 2.6
Peak current, pA	$-12.4 \pm 0.9^{(1*)}$	$-412 \pm 113^{(13*)}$	$-0.57 \pm 0.06^{(1*)}$	$-12 \pm 1.1^{(2*)}$	$-216 \pm 62^{(23*)}$	-0.5 ± 0.04
Eventarea (AOC), pC	$-0.51 \pm 0.7^{(1*)}$	$-37.7 \pm 11.5^{(13*)}$	$-0.34 \pm 0.06^{(4*)}$	$-0.60 \pm 0.05^{(2*)}$	$-20.1 \pm 7.0^{(23*)}$	$-0.28 \pm 0.05^{(4*)}$
$T_{weighted}$ (AOC/Peak)	$39.5 \pm 5.5^{(1*)}$	$72.7 \pm 8.5^{(13*)}$	49.6 ± 7.9	47.6 ± 6.0	59.6 ± 7.1	47.3 ± 10.9
T_{fitted}	$35.3 \pm 5.5^{(1*)}$	$66.3 \pm 9.4^{(1*)}$	$53.5 \pm 10.8^{(4*)}$	45 ± 5.8	71.6 ± 8.7	$47.2 \pm 8.1^{(4*)}$

Values are means $\pm$ SE of 6 cells (whole cell—spontaneous and evoked) and 6 slices (field). Effects of ifenprodil were assessed in the period of 5–10 min after application. Significant differences was determined using a paired *t*-test with level of significance at 0.05 between spontaneous and evoked in the same cell for the control [1*] and the ifenprodil period [2*], between evoked in the two periods [3*], and between fields in the two periods [4*].
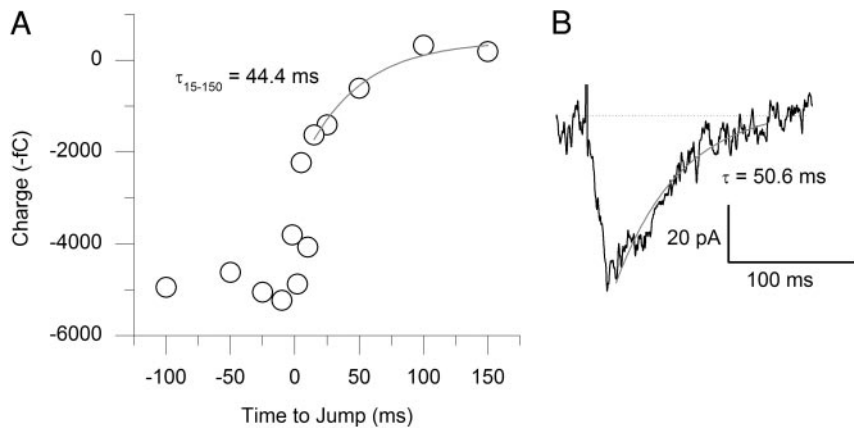
FIG. 6. Voltage jump from the reversal potential ($+3$ mV) to -60 mV at 11 different times relative to stimulation in site 1. *A*: the charge (AOC) recovered when stimulation occurs from -150 to $+100$ ms relative to the jump. The rise time of events are 16.2 ± 2.4 ms (see *B*) and fitting a single exponential to the charge recovered from jumps 15–150 ms before the jump is comparable to the decay time constant of events recorded 100 ms after the jump (i.e., at -60 mV). *B*: event recorded 100 ms after the jump. The decay time constant is comparable (see RESULTS) to that obtained in the charge recovery graph (see *A*).

with a lower expression of NR2D while NR2C is absent (Dunah et al. 1996; Fritschy et al. 1998; Monyer et al. 1994; Watanabe et al. 1993; Wenzel et al. 1995). NR2A and NR2B receptors are kinetically indistinguishable—they possess both high (50–60 pS) and low ($\sim$38 pS) conductance states, dependent on temperature, extracellular Mg^{2+} and Ca^{2+} concentrations and recording configuration (whole cell vs. single channel/patch) (Clark et al. 1997; Cull-Candy et al. 1998; Gibb and Colquhoun 1992; Lieberman and Mody 1994; Stern et al. 1994). NR2D receptors possess two lower conductance-levels at 42 and 19 pS (Cull-Candy et al. 1998). The application of NSFA presumes that two conditions are met regarding the composition of the channel-type and kinetics underlying the events. These basic assumptions derived from the binomial formulation of NSFA (Sigworth 1980) are that the kinetics of the N channels shaping the event are independent from each other and these N channels have a single conductance level during openings. The second of these conditions are not nec-

essarily met here because NMDA channels possess distinct subconductance levels (Clark et al. 1997; Cull-Candy et al.1998; Gibb and Colquhoun 1992; Stern et al. 1994). The estimate of the conductance obtained here is therefore only a weighted average of the different conductance levels of a presumably heterogeneous NMDA receptor population, which nevertheless remains a reasonable characterization of the weighted mean channel conductance. Our estimate of the channel conductance $\sim$60 pS (table 1, $n = 17$) is similar to that determined at room temperature by Traynelis et al. (1993) of 56–65 pS and to that of Clark et al. (1997) of 59 pS both using whole cell recordings of cerebellar granule cells, a preparation mainly containing NR2B receptors (Cull-Candy et al. 1998). Considering the increased channel conductance with temperature, our estimate recorded at 34°C appears comparatively low. The reason for the discrepancy will have to be determined by future studies, but it may be due to the synaptic localization of the channels. The ratio of average peak to single channel
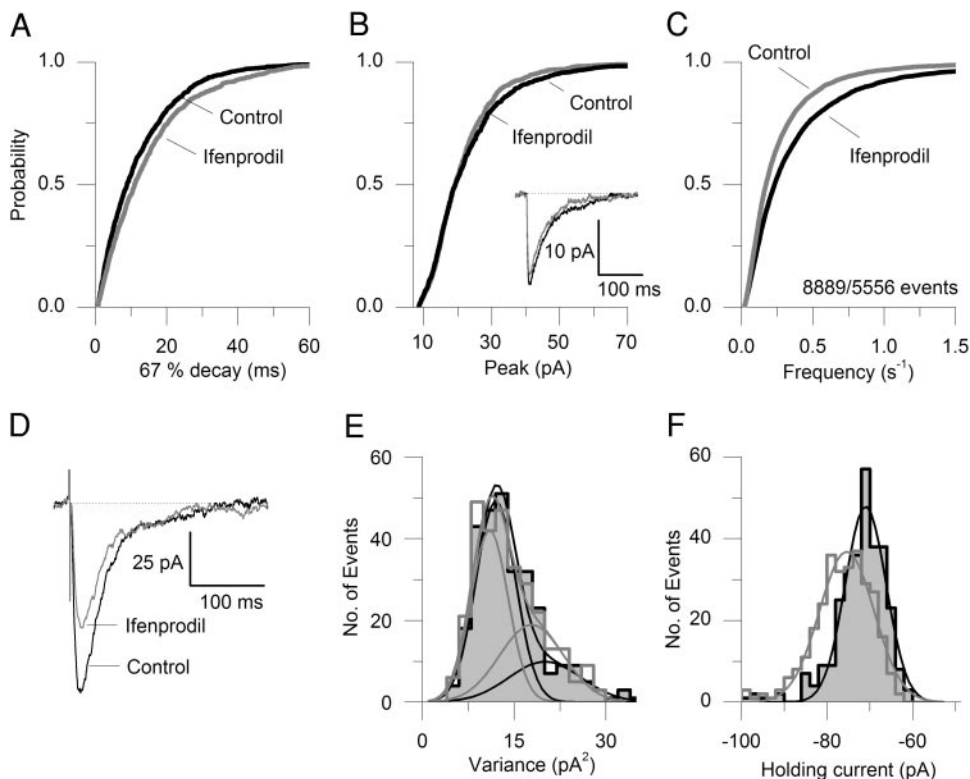

FIG. 7. Ifenprodil (10 μM) has no effect on basic properties of spontaneous NMDA receptor-mediated EPSCs. *A* and *B*: cumulative probability plots of 63% decay times and peak amplitudes, respectively. *Inset*: the average of spontaneous events from control and ifenprodil. *C*: cumulative probability plot of the interevent intervals showing a reduced frequency of events in ifenprodil. *D*: the average evoked NMDA EPSCs recorded during control (black) and in ifenprodil (gray). *E*: the distribution of the baseline current variance is unchanged by ifenprodil as is the holding current (*F*). Its mean value ($\pm$SE) is -47.0 ± 18.0 pA in control and -51 ± 12.0 pA in ifenprodil.
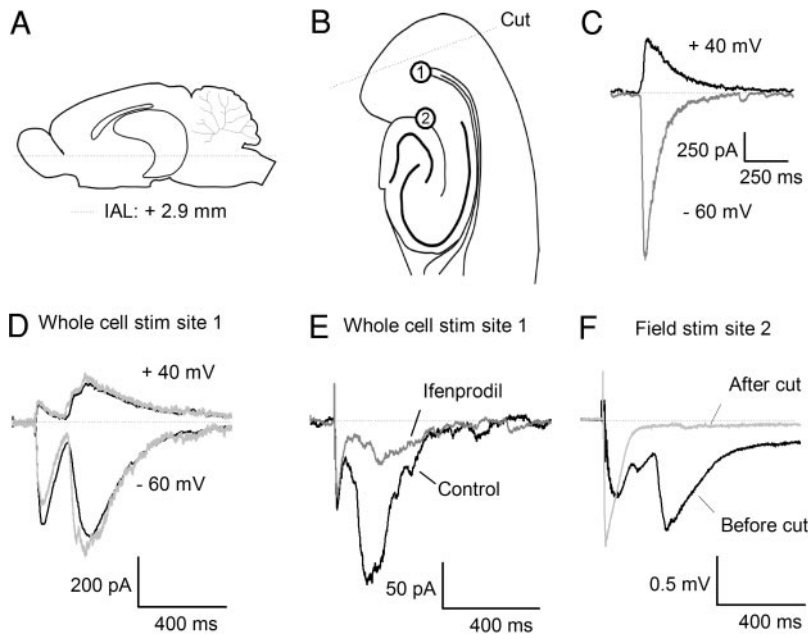
FIG. 8. NMDA receptor-mediated events in slices obtained from the ventral hippocampus, at a level ~2–3 mm above the interaural (IAL) line. *A*: sagital view of the rat brain and the approximate location of 2.9 mm above IAL is indicated (···). *B*: horizontal view of the hippocampus, subiculum, and medial and lateral entorhinal cortex at IAL = 2.9 mm (adapted from Paxinos and Watson 1998). The locations (1) of the stimulating electrode for whole cell recordings and for field recordings (2) are indicated. In some of the experiments, the entorhinal cortex was severed from the slice by a cut along the ··· while recording field potentials. *C*: large NMDA receptor-mediated spontaneous events were frequently encountered in ventral slices, but never in dorsal slices. This type of event was ~2 orders of magnitude larger in amplitude than "normal" spontaneous events in the same slices, or those recorded in dorsal slices, and reversed polarity at positive holding potentials. *D*: in ventral slices stimulus evoked events invariably gave rise to secondary peaks, which also reversed polarity at positive holding potentials. *E*: the amplitude of the secondary peak is much reduced in ifenprodil. *F*: average of 8 field potentials before and after a cut made to remove the entorhinal cortex.

current yields an estimate of ~4 channels open at the peak of spontaneous events (Table 1), a small number compared with ~40–50 channels open at the peak of spontaneous $GABA_A$ receptor-mediated events (De Koninck and Mody 1994).

Differences between evoked and spontaneous events

Stimulus evoked events had two to three times larger peak amplitudes than spontaneous events but showed more cell-to-cell variation in peak amplitude than spontaneous events. This is most likely due to variations in required stimulus strength and to a variable connection between EC afferents en passage the site of stimulation and the dendrites of the recorded cell. The higher peak amplitude of evoked (−46.5 pA) as compared with spontaneous events (−13.2 pA) most likely results from the activation of an additional number of release sites by the stimulated fiber(s) on the recorded cell. The long rise time of stimulus evoked events (peak-smoothing) may arise from the addition of several embedded components (see also Traynelis et al. 1993): evoked stimuli cause vesicle release through the activation of multiple release sites and possibly also by asynchronous release of multiple quanta from single release sites. Both situations would lead to an asynchrony in activation of postsynaptic receptors and thus a skew toward longer rise times. However, staggering of spontaneous events to match rise time and peak amplitude of the evoked event in the same cell show that when evoked from site 1, but not site 2 (different slice), kinetics of spontaneous and evoked NMDA EPSCs are comparable (Fig. 5, *A* and *B*). Although it is possible to closely replicate an average evoked event from the staggered addition of average spontaneous events (Fig. 5*A*), it should not be assumed that evoked events are merely a scale-up (summation) of spontaneous events. For example, the population of synapses giving rise to spontaneous events may not be identical to the synapses activated by stimulation since the perforant path contacts granule cells monosynaptically only in the outer two thirds of the dendritic tree.

Furthermore, an average event is an average of single spontaneous events from a distribution usually best described as being log-normal (see also Figs. 2, *B* and *C*, and 3, *B* and *C*). It is probably an oversimplification to assume that events from activated synapses along the outer two-thirds of the granule cell dendritic tree follow a similar distribution. As outlined in the preceding text, the synapses giving rise to spontaneous and evoked events might be anatomically distinct, and for evoked events, on average may be more distal. Voltage escape at distant synapses and slow onset-kinetics (like NMDA channels) can lead to serious distortion of rise time, peak current, and decay time measured at the soma, whereas the charge recovered at the soma is much less affected. To ascertain that the evoked events are not merely a filtered version of the spontaneous events, we employed the voltage jump/charge recovery method (Hausser and Roth 1997; Pearce 1993). Figure 6, *A* and *B,* shows how the charge recovery can reconstruct the true decay time constant of evoked events, yielding a value comparable to that of spontaneous events. Therefore the kinetics of evoked and spontaneous events faithfully reflect the true time course of synaptic NMDA channel conductance.

Evoked events from stimulation in site 2 (Fig. 6*B*, recorded in whole cell) have similar rise times to the events evoked from site 1 but larger peak amplitudes (−413 ± 113 pA) and significantly longer decay time constants compared with spontaneous events in the same cell (Table 3, $\tau_{weighted}$ = 66.3 ± 9.4). This larger decay time constant may be due to the activation of a set of receptors by spillover of glutamate or perhaps stimulation of synapses in the inner molecular layer (i.e., from secondarily activated mossy cells) not activated during spontaneous activity or by "minimal" stimulation from the more distant site 2.

Role of NR2B receptors

Ifenprodil is a noncompetitive inhibitor of NMDA receptors with a >400-fold selectivity for NR2B over that of NR2A

(Williams 1993) with a mechanism of action related to the proton-mediated inhibition of NMDA receptors. We found that ifenprodil had no effect on any measured parameter of spontaneous events, except their frequency (Table 2, Fig. 7, *A–F*). In field potentials and evoked whole cell currents ifenprodil caused a ~40% reduction in peak amplitude and charge carried by the event (Table 2). The differential effect of an NR2B antagonist on spontaneous and evoked events raises some questions about the differential distribution of NR2A and NR2B receptors. Ultrastructural studies employing immunogold labeled antisera recognizing extracellular epitopes concluded that NR1 is localized on the spine of 98–99% of asymmetric profiles at Schaffer-collateral synapses in the CA1 (Racca et al. 2000; Takumi et al. 1999a,b) and in the dentate gyrus outer molecular layer (Milner and Drake 2001). These studies also reported NR1 labeling of a few presynaptic profiles in both regions, but in the dentate, these were shown to be mainly associated with μ-opiod receptor containing fibers establishing symmetric contacts on granule cell dendrites (Milner and Drake 2001). However, because it has been argued that a detailed analysis of presynaptic NR1 localization requires the use of antibodies recognizing intracellular epitopes (Paquet and Smith 2000; Racca et al. 2000), a cautious conclusion is that NR1 is either not expressed or is expressed at below detection levels (using extracellular epitope recognizing antisera) in terminals at asymmetric synapses in the molecular layer. Unfortunately, ultrastructural analyses of NR2 receptors are not subtype specific, but functional studies from various synaptic preparations including hippocampal CA3–CA1 Schaffer-collaterals supports a picture of predominantly synaptically localized NR2A receptors with a largely extrasynaptic spread of NR2B receptors (Chen and Diamond 2002; Diamond 2001; Isaacson 1999; Kullman et al. 1999; Tovar and Westbrook; 1999) in which the timing of their activation is proportional to their distance from the presynaptic release site (Barbour and Hausser 1997; Takumi et al. 1999). However, two functional studies also support a presynaptic localization of NMDA receptors at hippocampal excitatory synapses (Breukel et al. 1998) and more specifically of NR2B receptors in a localized excitatory circuit in the entorhinal cortex (Woodhall et al. 2001). The possibility exists that heterotrimeric receptors (for example NR1/NR2A/NR2B) are expressed at synapses in adult rat dentate gyrus granule cells because there is good evidence for such receptors in recombinant expression systems (Brimecombe et al. 1997; Cheffings and Colquhoun 2000; Chen et al. 1997; Vicini et al. 1998). At present, evidence for the existence of heterotrimeric receptors in vivo comes from an NR1/NR2B/NR2D receptor combination expressed in P0 dentate granule cells (Pina-Crispo and Gibb 2002). Although the NR2B and NR2D receptor subunits are both considered to be predominantly extrasynaptic, we cannot rule out the existence of a NR1/NR2A/NR2B receptor combination at dentate granule cell synapses. This might be supported by comparing the decay kinetics of NMDA receptors in recombinant systems with the synaptic currents recorded by us. Although NR2A and NR2B receptors display similar channel conductance, activation studies of expressed receptors show marked differences in decay kinetics (Brimecombe et al. 1997; Chen et al. 1997; Vicini et al. 1998). Moreover, presumed NR1/NR2A/NR2B receptors displayed decay kinetics and pharmacological sensitivity intermediate between those of NR2A and NR2B receptors. Based

on the kinetic model of Chen et al. (2001), we have calculated the time constant at 32°C of the decay of a population of NR2A ($\tau = 16.5$ ms) and NR2B ($\tau = 122.6$ ms) receptors (rate constants are as described by Chen et al. 2001) (Table 1, using a Q10 of 2.5). Both values are about threefold off from the τ_{decay} of the synaptic events of 41.1 ms measured by us, and it may be that the difference stems from a mixed population of synaptic NR1/NR2A and NR1/NR2A/NR2B receptors. However, synaptic NMDA receptors are subject to modulation by a number of intracellular proteins, kinases and phosphatases, cytoskeleton anchoring proteins and Ca^{2+}-activated modulators, each of which have been shown to affect NMDA receptor properties. Such intracellular regulation at the synapse is not reflected by the modeled data or by recombinant expression systems thus making difficult the accurate comparisons with the properties of receptors at intact synapses.

In line with the potential NMDA receptor localization and composition at granule cell synapses, there might be several explanations for the effect of ifenprodil: the activity of layer II stellate neurons in the EC, the neurons that target granule cells, may be under the strict control of an NR2B receptor controlled excitatory circuit (Woodhall et al. 2001) leading to an ifenprodil-induced diminished activity in the entire EC-dentate gyrus circuitry. Ifenprodil may act presynaptically on NR2B receptors or N-type Ca^{2+} channels (Bath et al. 1996) to reduce presynaptic Ca-influx and hence release probability leading to a diminished frequency of spontaneous events. However, the reduction of presynaptic Ca^{2+} entry through voltage-gated channels by 10 μM ifenprodil is unlikely given the lower affinity of the drug for Ca^2 channels (Bath et al. 1996) than for NR2B receptors (Williams 1993). In light of the overlapping amplitude distributions of the spontaneous events recorded before and after ifenprodil administration (Fig. 7*B*), it is unlikely that the decreased frequency seen in ifenprodil was the result of smaller amplitude events having been driven into the noise. Furthermore, based on the longer deactivation times of NR2B compared with NR2A receptors, which would result in a longer decay of the synaptic currents, the unaltered decay times recorded under control conditions and in the presence of ifenprodil (Fig. 7*A*) argue against the presence of synaptic NR2B receptors. Based on the unaltered kinetics of the spontaneous events in the presence of ifenprodil, glutamate release by spontaneous action potentials is not sufficient to spillover and activate extrasynaptic NR2B receptors, i.e., NR2B receptors do not participate in shaping the spontaneous NMDA EPSCs at granule cell synapses. The presence of NR2B receptors at postsynaptic densities may also be regulated, and such receptors may not be in use during spontaneous activity. Stimulus-evoked events and field potentials cause the near-simultaneous activation of multiple synapses and may spillover glutamate to neighboring synapses. Surprisingly, the decay time constant of evoked responses from sites 1 and 2 (whole cell) was unchanged by ifenprodil (Tables 2 and 3), suggesting that the increased glutamate release during these two types of evoked responses does not selectively activate extrasynaptic NR2B receptors. However, ifenprodil caused a reduction in both the peak and decay time constant of NMDA field EPSPs, suggesting that under these conditions, extrasynaptic NR2B receptors are activated by overspill of glutamate. The discrepancy between data in these three different preparations presumably stems from the much higher stimulus strengths and

the proximity of the stimulating electrode required for evoking field EPSPs rather than EPSC. We cannot exclude the possibilities that NR2B receptor-mediated responses specifically ran down in whole cell recordings or that an ifenprodil effect at presynaptic EC layer II afferents will likely increase the number of failures during stimulation and thus reduce the number of activated granule cell synapses.

Synaptic bursting in ventral slices

Spontaneous and evoked events in ventral slices with amplitudes of ~2 orders of magnitude larger than mean peak in dorsal slices are NMDA receptor mediated based on their reversal at positive holding potentials (Fig. 8, *C* and *D*) and APV and ifenprodil sensitivity (Fig. 8*E*). Ventral slices also displayed spontaneous field potentials, while evoked fields were composed of double peaks dependent on an intact perforant path (Fig. 8*F*). Future studies will need to examine this phenomenon in more detail. At present, we note that the ventral hippocampus and EC possess several characteristics, each of which may contribute to the generation of these events. First, the presence of supragranular mossy fibers is frequently seen in control animals in this region (Buckmaster and Dudek 1997), which may increase excitability under these recording conditions. Second, horizontal slices from the ventral rather than dorsal hippocampus presumably contain more intact connections between layer two-three EC neurons and dentate granule cells (i.e., perforant path). Yet the angle of slicing may not be the only explanation because it is well established that the ventral hippocampus in vivo is much more excitable than the dorsal hippocampus, e.g., during kindling (Lerner-Natoli 1984).

Summary

We have provided the first characterization of spontaneous NMDA receptor-mediated synaptic events at granule cell synapses and demonstrated a dorsoventral difference in these events. The two stimulation sites investigated here show that evoked events from the EC/subiculum border better approximate kinetic parameters of spontaneous events than those evoked by stimulating near the hippocampal fissure. Using ifenprodil we have shown that NR2B receptors do not contribute to the spontaneous NMDA receptor-mediated EPSCs at granule cell synapses but regulate their frequency. The synaptic NMDA receptor aggregates predominantly contain NR2A with a possible contribution of NR2A/NR2B receptors. It remains to be determined whether the NR2B antagonist ifenprodil exerts its frequency-reducing effect at synapses through a reduction in the NR2B receptor controlled excitability in a local EC circuit thus reducing the output of the EC or alternatively via a presynaptic NR2B receptor on EC layer II afferents terminating in the molecular layer.

REFERENCES

Barbour B and Hausser M. Intersynaptic diffusion of neurotransmitter. *Trends Neurosci* 20: 377–384, 1997.

Bath CP, Farrell LN, Gilmore J, Ward MA, Hicks CA, O'Neill MJ, and Bleakman D. The effects of ifenprodil and eliprodil on voltage-dependent Ca^{2+} channels and in gerbil global cerebral ischaemia. *Eur J Pharmacol* 299: 103–12, 1996.

Brimecombe JC, Boeckman FA, and Aizenman E. Functional consequences of NR2 subunit composition in single recombinant *N*-methyl-D-aspartate receptors. *Proc Natl Acad Sci USA* 94: 11019–11024, 1997.

Breukel AI, Besselsen E, Lopes da Silva FH, and Ghijsen WE. A presynaptic *N*-methyl-D-aspartate autoreceptor in rat hippocampus modulating amino acid release from a cytoplasmic pool. *Eur J Neurosci* 10: 106–114, 1998.

Buckmaster PS and Dudek FE. Neuron loss, granule cell axon reorganization, and functional changes in the dentate gyrus of epileptic kainate-treated rats. *J Comp Neurol* 385: 385–404, 1997.

Chan SF and Sucher NJ. An NMDA receptor signaling complex with protein phosphatase 2A. *J Neurosci* 21: 7985–7992, 2001.

Cheffings CM and Colquhoun D. Single channel analysis of a novel NMDA channel from *Xenopus* oocytes expressing recombinant NR1a, NR2A and NR2D subunits. *J Physiol* 526: 481–491, 2000.

Chen N, Moshaver A, and Raymond LA. Differential sensitivity of recombinant *N*-methyl-D-aspartate receptor subtypes to zinc inhibition. *Mol Pharmacol* 51: 1015–1023, 1997.

Chen N, Ren J, Raymond LA, and Murphy TH. Changes in agonist concentration dependence that are a function of duration of exposure suggest *N*-methyl-D-aspartate receptor nonsaturation during synaptic stimulation. *Mol Pharmacol* 59: 212–219, 2001.

Chen S and Diamond JS. Synaptically released glutamate activates extrasynaptic NMDA receptors on cells in the ganglion cell layer of rat retina. *J Neurosci* 22: 2165–2173, 2002.

Clark BA, Farrant M, and Cull-Candy SG. A direct comparison of the single-channel properties of synaptic and extrasynaptic NMDA receptors. *J Neurosci* 17: 107–116, 1997.

Clark BA and Cull-Candy SG. Activity-dependent recruitment of extrasynaptic NMDA receptor activation at an AMPA receptor-only synapse. *J Neurosci* 22: 4428–4436, 2002.

Cull-Candy SG, Brickley SG, Misra C, Feldmeyer D, Momiyama A, and Farrant M. NMDA receptor diversity in the cerebellum: identification of subunits contributing to functional receptors. *Neuropharmacology* 37: 1369–1380, 1998.

De Koninck Y and Mody I. Noise analysis of miniature IPSCs in adult rat brain slices: properties and modulation of synaptic GABA$_A$ receptor channels. *J Neurophysiol* 71: 1318–1335, 1994.

Diamond JS. Neuronal glutamate transporters limit activation of NMDA receptors by neurotransmitter spillover on CA1 pyramidal cells. *J Neurosci* 21: 8328–8338, 2001.

Dunah AW, Yasuda RP, Wang YH, Luo J, Davila-Garcia M, Gbadegesin M, Vicini S, and Wolfe BB. Regional and ontogenic expression of the NMDA receptor subunit NR2D protein in rat brain using a subunit-specific antibody. *J Neurochem* 67: 2335–2345, 1996.

Fritschy JM, Weinmann O, Wenzel A, and Benke D. Synapse-specific localization of NMDA and GABA(A) receptor subunits revealed by antigen-retrieval immunohistochemistry. *J Comp Neurol* 390: 194–210, 1998.

Gibb AJ and Colquhoun D. Activation of *N*-methyl-D-aspartate receptors by L-glutamate in cells dissociated from adult rat hippocampus. *J Physiol* 456: 143–179, 1992.

Gordey M, Mekmanee L, and Mody I. Altered effects of ethanol in NR2A(DeltaC/DeltaC) mice expressing C-terminally truncated NR2A subunit of NMDA receptor. *Neuroscience* 105: 987–997, 2001.

Hardingham GE, Fukunaga Y, and Bading H. Extrasynaptic NMDARs oppose synaptic NMDARs by triggering CREB shut-off and cell death pathways. *Nat Neurosci* 5: 405–414, 2002.

Hausser M and Roth A. Estimating the time course of the excitatory synaptic conductance in neocortical pyramidal cells using a novel voltage jump method. *J Neurosci* 17: 7606–7625, 1997.

Hestrin S, Nicoll RA, Perkel DJ, and Sah P. Analysis of excitatory synaptic action in pyramidal cells using whole cell recording from rat hippocampal slices. *J Physiol* 422: 203–225, 1990.

Isaacson JS. Glutamate spillover mediates excitatory transmission in the rat olfactory bulb. *Neuron* 23: 377–384, 1999.

Krupp JJ, Vissel B, Thomas CG, Heinemann SF, and Westbrook GL. Calcineurin acts via the C-terminus of NR2A to modulate desensitization of NMDA receptors. *Neuropharmacology* 42: 593–602, 2002.

Kullmann DM, Min MY, Asztely F, and Rusakov DA. Extracellular glutamate diffusion determines the occupancy of glutamate receptors at CA1 synapses in the hippocampus. *Philos Trans R Soc Lond B Biol Sci* 354: 395–402, 1999.

Laube B, Kuhse J, and Betz H. Evidence for a tetrameric structure of recombinant NMDA receptors. *J Neurosci* 18: 2954–2961, 1998.

Lerner-Natoli M, Rondouin G, and Baldy-Moulinier M. Hippocampal kindling in the rat: intrastructural differences. *J Neurosci Res* 12: 101–111, 1984.

Lester RA, Clements JD, Westbrook GL, and Jahr CE. Channel kinetics determine the time course of NMDA receptor-mediated synaptic currents. *Nature* 346: 565–567, 1990.

Lieberman DN and Mody I. Regulation of NMDA channel function by endogenous Ca(2+)-dependent phosphatase. *Nature* 369: 235–239, 1994.

Lozovaya NA, Kopanitsa MV, Boychuk YA, and Krishtal OA. Enhancement of glutamate release uncovers spillover-mediated transmission by *N*-methyl-D-aspartate receptors in the rat hippocampus. *Neuroscience* 91: 1321–1330, 1999.

Milner TA and Drake CT. Ultrastructural evidence for presynaptic mu opioid receptor modulation of synaptic plasticity in NMDA-receptor-containing dendrites in the dentate gyrus. *Br Res Bull* 54: 131–140, 2001.

Momiyama A. Distinct synaptic and extrasynaptic NMDA receptors identified in dorsal horn neurons of the adult rat spinal cord. *J Physiol* 523: 621–628, 2000.

Monyer H, Sprengel R, Schoepfer R, Herb A, Higuchi M, Lomeli H, Burnashev N, Sakmann B, and Seeburg PH. Heteromeric NMDA receptors: molecular and functional distinction of subtypes. *Science* 256: 1217–1221, 1992.

Paquet M and Smith Y. Presynaptic NMDA receptor subunit immunoreactivity in GABAergic terminals in rat brain. *J Comp Neurol* 423: 330–347, 2000.

Paxinos G. and Watson C. *The Rat Brain in Stereotaxic Coordinates* (4th ed.). New York: Academic, 1998.

Pearce RA. Physiological evidence for two distinct GABA$_A$ responses in rat hippocampus. *Neuron* 10: 189–200, 1993.

Pina-Crespo JC and Gibb AJ. Subtypes of NMDA receptors in new-born rat hippocampal granule cells. *J Physiol* 541: 41–64, 2002.

Racca C, Stephenson FA, Streit P, Roberts JD, and Somogyi P. NMDA receptor content of synapses in stratum radiatum of the hippocampal CA1 area. *J Neurosci* 20: 2512–2522, 2000.

Rumbaugh G and Vicini S. Distinct synaptic and extrasynaptic NMDA receptors in developing cerebellar granule neurons. *J Neurosci* 19: 10603–10610, 1999.

Sattler R, Xiong Z, Lu WY, MacDonald JF, and Tymianski M. Distinct roles of synaptic and extrasynaptic NMDA receptors in excitotoxicity. *J Neurosci* 20: 22–33, 2000.

Sigworth FJ. The variance of sodium current fluctuations at the node of Ranvier. *J Physiol* 307: 97–129, 1980.

Staley KJ and Mody I. Integrity of perforant path fibers and the frequency of action potential independent excitatory and inhibitory synaptic events in dentate gyrus granule cells. *Synapse* 9: 219–224, 1991.

Stern P, Cik M, Colquhoun D, and Stephenson FA. Single channel properties of cloned NMDA receptors in a human cell line: comparison with results from *Xenopus* oocytes. *J Physiol* 476: 391–397, 1994.

Takumi Y, Matsubara A, Rinvik E, and Ottersen OP. The arrangement of glutamate receptors in excitatory synapses. *Ann NY Acad Sci* 868: 474–482, 1999a.

Takumi Y, Ramirez-Leon V, Laake P, Rinvik E, and Ottersen OP. Different modes of expression of AMPA and NMDA receptors in hippocampal synapses. *Nat Neurosci* 2: 618–624, 1999b.

Tovar KR and Westbrook GL. The incorporation of NMDA receptors with a distinct subunit composition at nascent hippocampal synapses in vitro. *J Neurosci* 19: 4180–4188, 1999.

Traynelis SF, Silver RA, and Cull-Candy SG. Estimated conductance of glutamate receptor channels activated during EPSCs at the cerebellar mossy fiber-granule cell synapse. *Neuron* 11: 279–289, 1993.

Vicini S, Wang JF, Li JH, Zhu WJ, Wang YH, Luo JH, Wolfe BB, and Grayson DR. Functional and pharmacological differences between recombinant *N*-methyl-D-aspartate receptors. *J Neurophysiol* 79: 555–566, 1998.

Watanabe M, Inoue Y, Sakimura K, and Mishina M. Distinct distributions of five *N*-methyl-D-aspartate receptor channel subunit mRNAs in the forebrain. *J Comp Neurol* 338: 377–390, 1993.

Wenzel A, Scheurer L, Kunzi R, Fritschy JM, Mohler H, and Benke D. Distribution of NMDA receptor subunit proteins NR2A, 2B, 2C, and 2D in rat brain. *Neuroreport* 7: 45–48, 1995.

Williams K. Ifenprodil discriminates subtypes of the *N*-methyl-D-aspartate receptor: selectivity and mechanisms at recombinant heteromeric receptors. *Mol Pharmacol* 44: 851–859, 1993.

Woodhall G, Evans DI, Cunningham MO, and Jones RS. NR2B-containing NMDA autoreceptors at synapses on entorhinal cortical neurons. *J Neurophysiol* 86: 1644–1651, 2001.

Wyllie DJ, Behe P, and Colquhoun D. Single-channel activations and concentration jumps: comparison of recombinant NR1a/NR2A and NR1a/NR2D NMDA receptors. *J Physiol* 510: 1–18, 1998.